

# Airway Labeling Meets Clinical Applications: Reflecting Topology Consistency and Abnormality via Learnable Attentions

Chenyu Li<sup>1,2</sup>, Minghui Zhang<sup>1,2</sup>, Chuyan Zhang<sup>1,2</sup>, Yun Gu<sup>1,2\*</sup>

<sup>1\*</sup>Institute of Medical Robotics, Shanghai Jiao Tong University,  
Shanghai, China.

<sup>2\*</sup>Institute of Image Processing and Pattern Recognition, Shanghai Jiao  
Tong University, Shanghai, China.

\*Corresponding author(s). E-mail(s): [yungu@ieee.org](mailto:yungu@ieee.org);

Contributing authors: [lichenyu@sjtu.com](mailto:lichenyu@sjtu.com); [minghuizhang@sjtu.edu.cn](mailto:minghuizhang@sjtu.edu.cn);  
[zhangchuyan@sjtu.edu.cn](mailto:zhangchuyan@sjtu.edu.cn);

## Abstract

**Purpose:** Accurate airway anatomical labeling is crucial for clinicians to identify and navigate complex bronchial structures during bronchoscopy. Automatic airway anatomical labeling is challenging due to significant individual variability and anatomical variations. Previous methods are prone to generate inconsistent predictions, which is harmful for preoperative planning and intraoperative navigation. This paper aims to address these challenges by proposing a novel method that enhances topological consistency and improves the detection of abnormal airway branches.

**Methods:** We propose a novel approach incorporating two modules: the Soft Subtree Consistency (SSC) and the Abnormal Branch Saliency (ABS). The SSC module constructs a soft subtree to capture clinically relevant topological relationships, allowing for flexible feature aggregation within and across subtrees. The ABS module facilitates the interaction between node features and prototypes to distinguish abnormal branches, preventing the erroneous aggregation of features between normal and abnormal nodes.

**Results:** Evaluated on a challenging dataset characterized by severe airway distortion and atrophy, our method achieves superior performance compared to state-of-the-art approaches. Specifically, it attains a 91.4% accuracy at the segmental level and an 83.7% accuracy at the subsegmental level, representing a

1.4% increase in subsegmental accuracy and a 3.1% increase in topological consistency. Notably, the method demonstrates reliable performance in cases with disease-induced airway deformities, ensuring consistent and accurate labeling.

**Conclusion:** The enhanced topological consistency and robust identification of abnormal branches provided by our method offers a reliable solution for airway labeling, with significant potential to improve both the effectiveness and safety of bronchoscopy procedures in clinical practice.

**Keywords:** Airway anatomical labeling, Structural prior, Anomaly detection

## 1 Introduction

Bronchial anatomical labeling enables clinicians to precisely identify the bronchus or subsegment involved with the pathological lesion, thereby facilitating the optimal planning of the surgical approach while minimizing injury to surrounding healthy tissues [1, 2]. When integrated with advanced navigation technologies, bronchial anatomical labeling supports the precise guidance of surgical instruments by robotic or navigational systems, ensuring accurate execution of procedures within the intricate pulmonary anatomy [3]. Furthermore, bronchial anatomical labeling also assists clinicians in better assessing individual anatomical variations in each patient and developing personalized surgical plans, particularly for patients with significant anatomical anomalies.

Manual annotation of bronchial anatomical labeling by medical experts is time-consuming and requires a high level of expertise. Different from the binary segmentation tasks [4], this task assigns the branches with specific class labels according to the anatomy. Therefore, automated labeling algorithms have emerged to alleviate the workload of clinicians. However, automatic bronchial anatomical labeling among different patients can be challenging from two aspects. Firstly, individual variability leads to substantial feature overlap, further aggravated by disease-induced airway deformities. Traditional algorithms rely on predefined rules [1, 5] or association graph search [6, 7], failing to accurately label distal branches. Recently, deep learning methods [8–10] have demonstrated superior performance on this task. To address individual differences, a hyper-graph model was introduced by [8] to encode subtree representations through hyperedges. However, it relies heavily on manually designed hypergraphs and is sensitive to hyperparameters. Xie *et al.* [10] encoded deep point-graph representation for analyzing 3D pulmonary tree structures, but only achieved segmental-level classification. AirwayFormer [9] was proposed to aggregate features using a self-attention mechanism and neighborhood encoding. Although these approaches achieved promising labeling results, limited attention has been paid to airway deformity such as atrophy, compression, and dilatation, resulting in failure in deformed airways as shown in Fig. 1(b). Secondly, the bronchial tree exhibits considerable morphological variability, with many anatomical variations beyond established nomenclatures. These abnormal branches without certain locations and orientations lack consistent anatomical descriptions, which complicates identification and impacts the classification of other

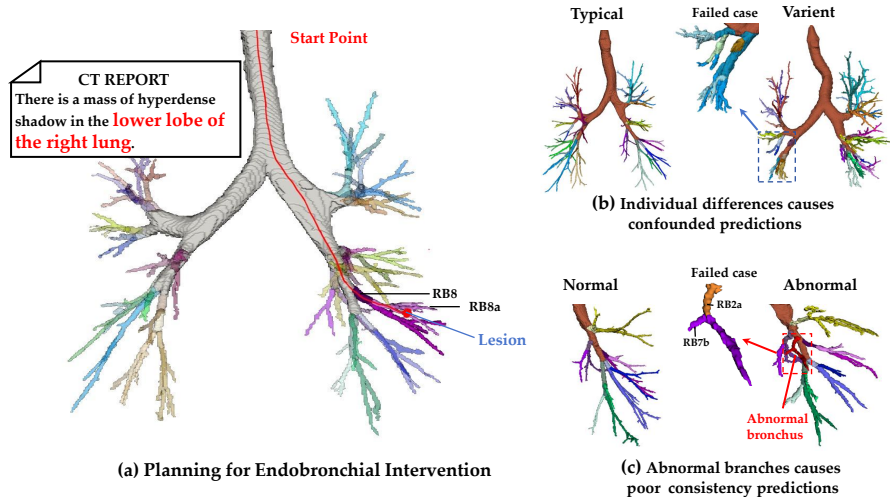


**Fig. 1** (a) illustrates the preoperative planning path for bronchoscopy. (b) and (c) shows that two main challenges will reduce clinical usability.

branches. However, current methods often overlook these variant branches. Huang *et al.* [11] treated abnormal bronchus as a separate category, while the absence of anatomical standards made it challenging to categorize them equally with other classes as illustrated in Fig. 1(c).

To alleviate the aforementioned challenges, we focus on the topological consistency for bronchial anatomical labeling. Specifically, we propose the Soft Subtree Consistency (SSC) module to tackle the first challenge, SSC constructs a soft subtree via feature interaction and topological refinement. Segmental labels serve as the criterion for soft subtrees, resulting in more flexible and discriminative feature aggregation within and across subtrees. To deal with the second challenge, we propose an Abnormal Branch Saliency (ABS) module, which compares node features and prototypes to predict anomaly scores, distinguishing abnormal nodes. And a soft mask derived from anomaly scores is utilized to prevent feature aggregation between normal and abnormal nodes for a smoother regularization.

The proposed method is evaluated on the AIIB23 [12] dataset, which is characterized by severe airway distortion and atrophy. Extensive experiments demonstrate that our method achieves superior performance compared to other state-of-the-art methods, achieving 91.4% accuracy in segmental, 83.7% accuracy in sub-segmental with a 1.4% increase, 96.8% consistency with a 3.1% increase, achieving consistent results in disease-induced airway deformities.

## 2 Method

Each airway branch is represented as a node in the graph, with attributes designed to reflect its location, morphology, and structure. An overview of the proposed method is illustrated in Fig. 2. We propose two modules to improve the consistency of prediction: (1) Soft Subtree Consistency (SSC) module (detailed in Section 2.2) softly encodes the

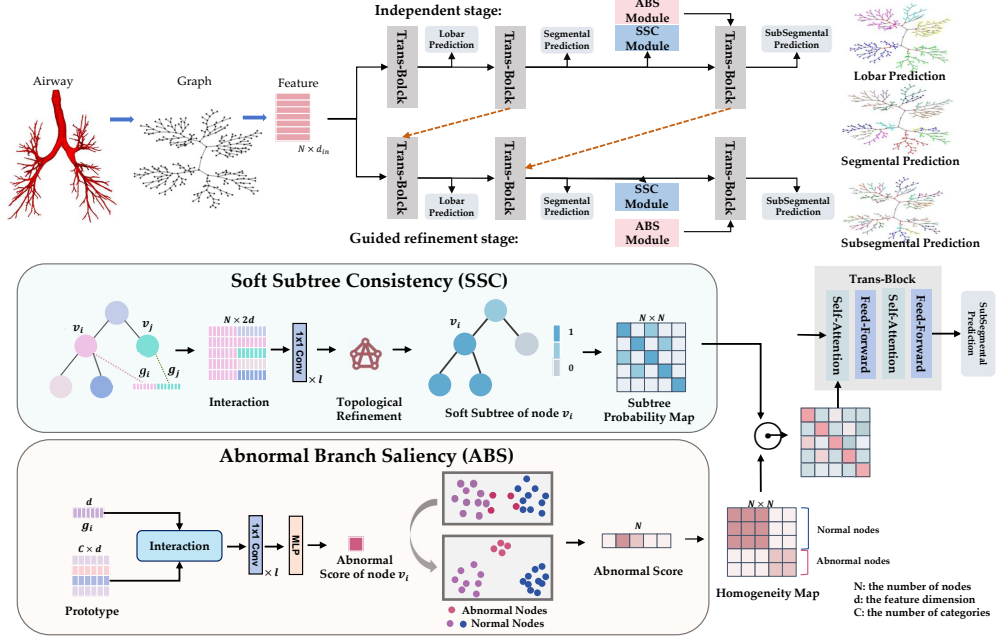


**Fig. 2** Overview of the proposed method: The airway labeling method comprises a Soft Subtree Consistency (SSC) module, which generates a soft subtree probability map, and an Abnormal Branch Saliency (ABS) module, which produces an abnormality score prediction. Both of them are used to inform attention interaction at the subsegmental level.

relationship between subtrees. (2) Abnormal Branch Saliency (ABS) module (detailed in Section 2.3) distinguishes between normal nodes and abnormal nodes.

## 2.1 Overall Framework

We adopt a U-shaped framework that progressively improves classification accuracy by incorporating hierarchical relationships. This framework comprises two stages: an independent stage (1st stage) and a guided refinement stage (2nd stage). The latter employs a fine-to-coarse guidance mechanism, using finer level features from the independent stage to refine coarser-level predictions, thereby enhancing overall labeling performance.

In the  $i$ -th ( $i = 1, 2$ ) stage, where the 1st one denotes the independent stage, and the 2nd one denotes the guided refinement stage, airway classification tasks are refined through cascaded transformer blocks:

$$\begin{aligned} \tilde{G}_m^i &= \mathcal{F}(q = k = v = X_m^i), \\ G_m^i &= \begin{cases} \mathcal{F}(q = \tilde{G}_m^i, k = v = G_{m+1}^{i-1}) & \text{for } m \in \{\text{lob}, \text{seg}\} \text{ and } i = 2 \\ \tilde{G}_m^i & \text{otherwise} \end{cases}. \end{aligned} \quad (1)$$

Here, the hierarchical level  $m \in \mathcal{H}$ , where the ordered set  $\mathcal{H} = \{lob, seg, sub\}$  corresponding to lobar, segmental, and subsegmental levels respectively.  $\mathcal{F}$  denotes the function of Transformer architecture.  $X_m^i \in \mathbb{R}^{N \times d}$  and  $G_m^i \in \mathbb{R}^{N \times d}$  represent the input and output features of the  $m$ -th transformer block in the  $i$ -th stage, where  $N$  denotes the number of nodes and  $d$  is the feature dimension. For simplicity, we take the guided refinement stage for an example, omitting the index  $i$  in subsequent notation.

The Transformer Block serves as the backbone and aggregates information globally through the attention mechanism [13]. A graph bias term [14] is added to the attention map, incorporating topological information:

$$A_m = \frac{(X_m Q_m)(X_m K_m)^T}{\sqrt{d}} + B_m, \quad (2)$$

$Q_m \in \mathbb{R}^{d \times d_k}$  and  $K_m \in \mathbb{R}^{d \times d_k}$  denote the learnable attention parameters. We use  $\psi(v_i, v_j)$  as the shortest path distance (SPD) between node  $v_i$  and node  $v_j$ . The bias matrix  $B_m \in \mathbb{R}^{N \times N}$  is a learnable codebook indexed by  $\psi \in \mathbb{R}^{N \times N}$ .

The finer classification utilizes the output of the coarser level as input, inheriting shared information to reduce the classification difficulty. Additionally, due to the corresponding relationship of the hierarchical nomenclature, finer predictions can directly infer coarser ones. Thus, finer features from the independent stage serve as additional input to guide coarse-grained classification.

## 2.2 Soft Subtree Consistency

Due to significant inter-individual variability, relying solely on node representations for classification can lead to substantial feature overlap. To address this challenge, we propose the Soft Subtree Consistency (SSC) module, which encodes subtree representations. Unlike hard-subtree techniques that use the number of descendants as a criterion for subtree construction, we utilize segmental labels to define subtrees that convey clinically relevant anatomical meaning. The soft subtree map  $M_t \in \mathbb{R}^{N \times N}$  is introduced, where  $M_t(i, j)$  represents the probability that nodes  $v_i$  and  $v_j$  belong to the same subtree. The ground truth labels for  $M_t$  are defined as,

$$M_t(i, j) = \begin{cases} 1 & Y_{seg}(i) = Y_{seg}(j) \\ 0 & Y_{seg}(i) \neq Y_{seg}(j) \end{cases}, \quad (3)$$

where  $Y_{seg} \in \mathbb{R}^N$  denotes the segmental level label.

As segmental labels define subtrees, we utilize segmental feature  $G_{seg} = (g_1, g_2, \dots, g_N)^T \in \mathbb{R}^{N \times d}$  to infer the soft subtree map (as shown in Fig. 2). Taking node  $v_i$  as an example, its feature  $g_i$  interacts with the features of all the nodes, then processed by several  $1 \times 1$  convolutional layers to reduce dimensionality. Repeating this process for all nodes yields the soft subtree map  $\bar{M}_t$ . However, a hard subtree comprises a node and all its descendants. Similarly, to reflect this in our soft subtree, the probability of nodes  $v_i$  and  $v_j$  belonging to the same subtree should be increased

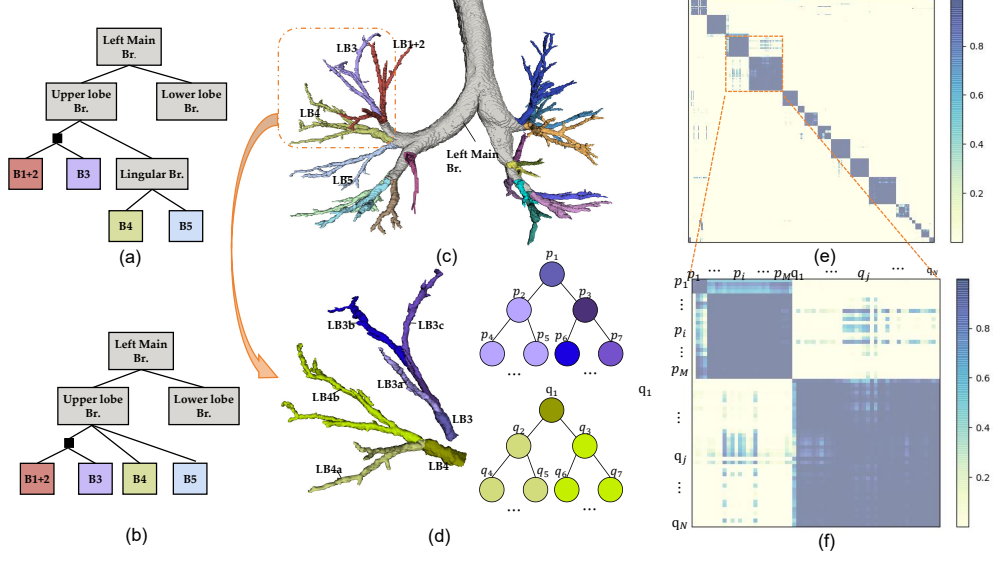


**Fig. 3** (a) illustrates the typical pattern of the left upper lobe, featuring a long lingular branch originating from the left main bronchus and bifurcating into LB4 and LB5. (b) shows a variant pattern where LB4 and LB5 directly bifurcates from the left main bronchus. (c) demonstrates a variant airway at the segmental level. (d) describes LB3 and LB4 at the subsegmental level. (e) shows the soft subtree map of the Airway. (f) details the Segment Consistency Mask

if  $v_j$  is a descendant of  $v_i$ . Hence, the soft topological refinement is defined as below:

$$\hat{M}_t = M_D \odot (\bar{M}_t + K(1 - \bar{M}_t)) + (1 - M_D) \odot \bar{M}_t,$$

$$M_D(i, j) = \begin{cases} 1 & v_j \in \mathcal{D}(v_i) \\ 0 & v_j \notin \mathcal{D}(v_i) \end{cases}, \quad (4)$$

where  $K \in [0, 1]^{N \times 1}$  is an learnable parameter.  $\mathcal{D}(v_i)$  denotes the set of all descendant nodes of node  $v_i$ .

According to the hierarchical nomenclature, the assignment of subsegmental labels is determined by their relative relationships to branches within a segment. The soft subtree map constrains feature aggregation within and across subtrees at the subsegmental level as follows,

$$A_{sub} = \frac{(X_{sub} Q_{sub})(X_{sub} K_{sub})^T}{\sqrt{d}} \odot \hat{M}_t, \quad (5)$$

The soft subtree map subsequently promotes the clustering of feature representations according to shared subtree characteristics. Subsequent attention layers calculated as Eq. (2) with global receptive fields then refine these representations, allowing for distinctions between individual nodes. This approach improves the clustering of subsegmental features by segmental category and simplifies the prediction

of subsegmental categories into encoding intra-subtree relations, effectively enhancing the accuracy and consistency of prediction.

An example of the mask is shown in Fig. 3. As illustrated, the positions and orientations of LB4 branches in this variant differ significantly from the typical pattern. LB4 exhibits greater positional and orientational similarity to LB3 than LB5, resulting in substantial feature overlap between LB3 and LB4. The mask generated by the SSC module limits feature aggregation between different segments, thereby alleviating feature overlap.

### 2.3 Abnormal Branch Saliency

The position, orientation, and shape of abnormal branches are uncertain, with significant individual differences. The primary criterion for identifying an abnormal branch is its inability to be classified into any category within the nomenclature. Thus, we propose an Abnormal Branch Saliency (ABS) that compares node features with class representations to detect anomalies. First, the class representation is obtained through the segmental features  $G_{seg} \in \mathbb{R}^{N \times d}$  and prediction logits  $Z_{seg} \in \mathbb{R}^{N \times C_{seg}}$ , where  $C_{seg}$  denotes the number of segment categories to obtain:

$$P_{seg} = \text{softmax}(Z_{seg}), \quad (6)$$

$$H = ((P_{seg})^\alpha)^T G_{seg}, \quad (7)$$

$P_{seg} \in [0, 1]^{N \times C_{seg}}$  denotes prediction probabilities.  $H \in \mathbb{R}^{C_{seg} \times d}$  are representations for segmental categories. Then they are refined through a transformer for improvement:

$$\tilde{H} = \mathcal{F}(q = H, k = v = G_{seg}). \quad (8)$$

Subsequent operations follow a similar process as the SSC module. Each pair of feature and prototypes is concatenated along the depth dimension, forming the  $\phi \in \mathbb{R}^{N \times C_{seg} \times 2d}$ .  $\phi$  is processed through several  $1 \times 1$  convolutional layers to reduce the depth dimension, followed by the Multilayer Perceptron (MLP).

Finally, the ABS module generates an anomaly score  $\hat{Y}_a \in [0, 1]^{N \times 1}$ , indicating the probability of each node being an abnormal branch. Due to the distinctive characteristics of abnormal branches, it is too absolute and arbitrary to use this anomaly score to directly classify nodes as a category equally with other classes. Instead, we generate a soft mask  $M_a \in \mathbb{R}^{N \times N}$  for smoother regularization, which prevents feature aggregation between normal and abnormal nodes:

$$\hat{M}_a = 1 - (\hat{Y}_a \hat{Y}_a^T)^2. \quad (9)$$

Mask  $\hat{M}_a$  guides abnormal nodes away from normal nodes in the feature space, aiding in more accurate predictions for normal nodes. Additionally, the abnormality score highlights potential abnormal branches and assists doctors in understanding the airway structure. Combining the two soft masks,  $\hat{M}_t \odot \hat{M}_a$  is applied to the attention

interaction of subsegmental Transformer Block,

$$A_{sub} = \frac{(X_{sub}Q_{sub})(X_{sub}K_{sub})^T}{\sqrt{d}} \odot (\hat{M}_t \odot \hat{M}_a), \quad (10)$$

For classification tasks, cross-entropy loss with label smoothing is used, excluding abnormal nodes from the loss calculation. Binary cross-entropy loss is employed for both soft subtree map  $\hat{M}_t$  prediction and abnormal score prediction  $\hat{Y}_a$ . The total loss function is formulated as:

$$\mathcal{L} = \sum_{i=1}^2 \gamma_i \left( \sum_{m \in \mathcal{H}} \alpha_m \mathcal{L}_{CE}(\hat{Y}_m^i, Y_m) + \beta_1 \mathcal{L}_{BCE}(\hat{M}_t^i, M_t) + \beta_2 \mathcal{L}_{BCE}(\hat{Y}_a^i, Y_a) \right), \quad (11)$$

where  $\gamma_i, \alpha_m, \beta_1, \beta_2$  are empirically tuned parameters.

## 3 EXPERIMENTS AND RESULTS

### 3.1 Datasets and implementation details

We used a subset of ATM22 [4] for training, selected based on the absence of significant airway deformities, with visibility extending two generations below the subsegmental level. The slice thicknesses were below 0.67 mm, and the spatial resolution ranged from 0.78 mm to 0.82 mm. And 89 cases were selected from the AIIB23 [12] dataset for verifying, exhibiting various airway abnormalities such as atrophy and distortion. Then we extracted the airway centerlines from segmentation results through the skeletonization algorithm [15], identifying bifurcation points to divide the airway into branches. We adopted a three-level nomenclature [16] for the bronchial tree, including 6 types of lobar bronchi, 19 types of segmental bronchi, and 127 types of subsegmental bronchi, with an additional "outlier" category for abnormal nodes.

The weight of loss function  $\gamma_i, \alpha_m, \beta_1,$  and  $\beta_2$  were set to 1. The label smoothing hyperparameter was set to 0.01. We employed the Adam optimizer for training with a learning rate of  $5e^{-4}$  over 600 epochs. For lobar and segmental airway labeling, we stacked two transformers calculated as Eq. (2). At the subsegmental level, we stacked two transformers calculated as Equation 10, followed by two more as Eq. (2). Finally, the predictions from the guided refinement stage served as the output.

### 3.2 Evaluation metrics and results

Five evaluation metrics are used to evaluate our method: consistency (CS), accuracy (ACC), precision (PR), recall (RC), and F1 score (F1). The consistency metric was developed to quantify clinical usability. This metric evaluates the anatomical uniformity of predictions for each node and its descendants at the segmental level, defined as the proportion of nodes meeting this criterion.



**Table 1** Quantitative comparison with different methods in airway anatomical labeling (%). The best result is in **BOLD**.

Method	Lobar				Segmental					Subsegmental			
	ACC	PR	RC	F1	CS	ACC	PR	RC	F1	ACC	PR	RC	F1
GCN[17]	91.7	92.0	89.1	89.0	60.4	67.3	59.6	68.7	55.1	45.5	30.5	35.4	29.5
GraphSAGE[18]	93.3	93.6	92.0	91.6	64.4	72.6	64.2	74.0	60.6	55.7	46.0	49.8	44.6
UniSAGE[19]	93.2	93.7	91.9	91.5	69.8	72.9	64.3	74.0	60.6	57.0	46.9	50.6	45.6
TNN[8]	95.3	93.9	94.0	93.2	85.4	78.7	65.2	77.9	64.4	63.3	50.6	57.0	50.9
AirwayFormer[9]	97.1	96.5	97.0	96.6	93.7	90.2	88.9	90.0	88.1	82.3	78.1	79.6	77.5
DeepAssign[20]	96.4	95.9	95.8	95.4	87.1	88.9	87.5	88.4	86.5	81.0	75.3	77.5	74.8
Ours	<b>97.4</b>	<b>96.9</b>	<b>97.2</b>	<b>96.8</b>	<b>96.8</b>	<b>91.4</b>	<b>89.0</b>	<b>90.2</b>	<b>88.5</b>	<b>83.7</b>	<b>79.1</b>	<b>80.9</b>	<b>78.6</b>

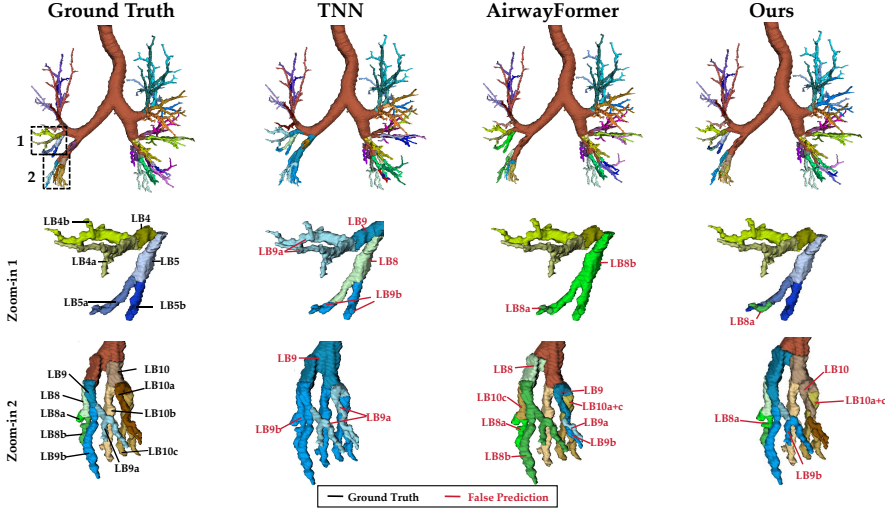


**Fig. 4** Qualitative results at subsegmental label for deformed airways. Ground truth of branches are in black, while false predictions of branches are in red. Our method demonstrates improved accuracy and consistency in predicting deformed airways.

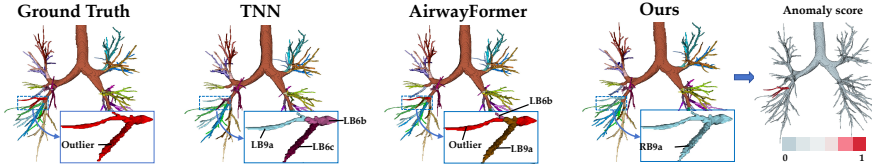


**Fig. 5** Qualitative results at subsegmental label for abnormal branches. Our method achieves superior performance.

Table 1 reports the quantitative results of our proposed method with other methods. For GNN methods such as GCN[17] and GraphSAGE[18], the one-hot neighborhood aggregation limited their ability to capture long-range topological relationships, resulting in poor classification accuracy, especially at subsegmental level.

**Table 2** Results (%) of ablation study of key components. F2C denotes network with fine-to-coarse guidance.

Method	Lobar				Segmental					Subsegmental			
	ACC	PR	RC	F1	CS	ACC	PR	RC	F1	ACC	PR	RC	F1
Baseline	96.8	96.0	96.4	95.8	87.9	89.2	87.7	88.7	85.7	81.2	76.0	78.1	75.4
F2C	97.2	96.7	97.1	96.6	94.3	90.6	89.3	90.2	88.5	82.7	78.4	80.0	77.9
F2C + SSC	97.4	97.1	97.2	96.8	95.7	90.8	88.2	89.5	87.6	83.2	78.5	80.2	78.0
F2C + ABS	<b>97.5</b>	<b>97.1</b>	97.2	<b>96.9</b>	94.1	91.1	<b>89.6</b>	<b>90.6</b>	<b>90.0</b>	83.4	78.8	80.7	<b>78.6</b>
F2C + SSC + ABS	97.4	96.9	<b>97.2</b>	96.8	<b>96.8</b>	<b>91.4</b>	89.0	90.2	88.5	<b>83.7</b>	<b>79.1</b>	<b>80.9</b>	<b>78.6</b>

For HGNN methods, UniSAGE[19] used hyperedges to encode subtree representations. TNN[8] leveraged a novel sub-network architecture for enhanced subtree communication, resulting in improved performance compared to other HGNN methods. For transformer method, the DeepAssign method[20], despite its flexible and differentiable label assignment, faced challenges in learning the complex structure inherent in a large number of subsegmental categories. AirwayFormer[9] leveraged attention mechanisms for global filed and encoded neighborhood information to capture tree structure priors. Compared with the above methods, our method demonstrated a 1.2% increase in segmental level accuracy, a 1.4% increase in subsegmental accuracy, and a remarkable 3.1% improvement in consistency, greatly enhancing clinical value.

Fig. 4 and Fig. 5 qualitatively demonstrate the superiority of our method. For disease-induced airway deformities, the subtrees constructed by the TNN method failed to reflect anatomical meaning, resulting in the misclassification of atrophied regions as the same label. AirwayFormer, which focuses on node-pair relationships without subtree encoding, suffers from inconsistent predictions. For abnormal branches, if they are classified equally with other classes, the absence of a standardized definition for these branches leads to inconsistent predictions. Our method consistently yields accurate predictions in both scenarios. For more details, please refer to the supplementary material.

### 3.3 Ablation study

Table. 2 reveals the effectiveness of each component in the proposed method. A baseline model consists of three cascaded transformer blocks. Fine-to-coarse guidance encodes the dependencies among the nomenclatures, and their interaction improves the classification results. The incorporation of the SSC module generates a soft subtree map that integrates anatomically relevant topological information, further enhancing performance, particularly a 1.4% increase in consistency. ABS module is effective to suppress the misclassification of the abnormal branches based on the anomaly scores, achieving 83.4% in subsegmental accuracy. The combined modules achieved the best performance, showing improvements of 2.2% in segmental accuracy, 2.5% in subsegmental accuracy, and 8.9% in consistency, thus validating the contribution of each component.

## 4 Conclusion

In this paper, an automated method for airway anatomical labeling is proposed. A soft subtree map, incorporating anatomically topological information, was introduced to softly encode subtree representations. Further, it effectively handled anomalous branches through the interaction between node features and prototypes. The superior performance on the AIIB23 dataset, particularly in consistency metrics, demonstrated the clinical potential of our approach.

## References

- [1] Mori, K., Hasegawa, J.-i., Suenaga, Y., Toriwaki, J.-i.: Automated anatomical labeling of the bronchial branch and its application to the virtual bronchoscopy system. *IEEE Transactions on medical imaging* **19**(2), 103–114 (2000)
- [2] Sitzwohl, C., Langheinrich, A., Schober, A., Krafft, P., Sessler, D.I., Herkner, H., Gonano, C., Weinstabl, C., Kettner, S.C.: Endobronchial intubation detected by insertion depth of endotracheal tube, bilateral auscultation, or observation of chest movements: randomised trial. *Bmj* **341** (2010)
- [3] Zhang, J., Fang, Q., Xiang, P., Xiong, R., Wang, Y., Lu, H.: Soft hybrid actuated hierarchical bronchoscope robot for deep lung examination. *IEEE Robotics and Automation Letters* **9**(1), 811–818 (2023)
- [4] Zhang, M., Wu, Y., Zhang, H., Qin, Y., Zheng, H., Tang, W., Arnold, C., Pei, C., Yu, P., Nan, Y., *et al.*: Multi-site, multi-domain airway tree modeling. *Medical image analysis* **90**, 102957 (2023)
- [5] Feragen, A., Petersen, J., Owen, M., Lo, P., Thomsen, L.H., Wille, M.M.W., Dirksen, A., Bruijne, M.: Geodesic atlas-based labeling of anatomical trees: Application and evaluation on airways extracted from ct. *IEEE transactions on medical imaging* **34**(6), 1212–1226 (2014)
- [6] Kitaoka, H., Park, Y., Tschirren, J., Reinhardt, J., Sonka, M., McLennan, G., Hoffman, E.A.: Automated nomenclature labeling of the bronchial tree in 3d-ct lung images. In: *Medical Image Computing and Computer-Assisted Intervention—MICCAI 2002: 5th International Conference Tokyo, Japan, September 25–28, 2002 Proceedings, Part II* 5, pp. 1–11 (2002). Springer
- [7] Juerg, T.: Matching and anatomical labeling of human airway tree. *IEEE Transactions on Medical Imaging* (2005)
- [8] Yu, W., Zheng, H., Gu, Y., Xie, F., Yang, J., Sun, J., Yang, G.-Z.: Tnn: Tree neural network for airway anatomical labeling. *IEEE Transactions on Medical Imaging* **42**(1), 103–118 (2022)

- [9] Yu, W., Zheng, H., Gu, Y., Xie, F., Sun, J., Yang, J.: Airwayformer: structure-aware boundary-adaptive transformers for airway anatomical labeling. In: International Conference on Medical Image Computing and Computer-Assisted Intervention, pp. 393–402 (2023). Springer
- [10] Xie, K., Yang, J., Wei, D., Weng, Z., Fua, P.: Efficient anatomical labeling of pulmonary tree structures via deep point-graph representation-based implicit fields. *Medical Image Analysis*, 103367 (2024)
- [11] Huang, W., Gong, H., Zhang, H., Wang, Y., Wan, X., Li, G., Li, H., Shen, H.: Bnet: Bronchus classification via structure guided representation learning. *IEEE Transactions on Medical Imaging* (2024)
- [12] Nan, Y., Xing, X., Wang, S., Tang, Z., Felder, F.N., Zhang, S., Ledda, R.E., Ding, X., Yu, R., Liu, W., *et al.*: Hunting imaging biomarkers in pulmonary fibrosis: Benchmarks of the aiib23 challenge. *Medical Image Analysis* **97**, 103253 (2024)
- [13] Vaswani, A.: Attention is all you need. *Advances in Neural Information Processing Systems* (2017)
- [14] Ying, C., Cai, T., Luo, S., Zheng, S., Ke, G., He, D., Shen, Y., Liu, T.-Y.: Do transformers really perform badly for graph representation? *Advances in neural information processing systems* **34**, 28877–28888 (2021)
- [15] Lee, T.-C., Kashyap, R.L., Chu, C.-N.: Building skeleton models via 3-d medial surface axis thinning algorithms. *CVGIP: graphical models and image processing* **56**(6), 462–478 (1994)
- [16] Netter, F.H.: Atlas of human anatomy, professional edition e-book: including netterreference. com access with full downloadable image bank (2014)
- [17] Kipf, T.N., Welling, M.: Semi-supervised classification with graph convolutional networks. *arXiv preprint arXiv:1609.02907* (2016)
- [18] Hamilton, W., Ying, Z., Leskovec, J.: Inductive representation learning on large graphs. *Advances in neural information processing systems* **30** (2017)
- [19] Ding, K., Wang, J., Li, J., Li, D., Liu, H.: Be more with less: Hypergraph attention networks for inductive text classification. *arXiv preprint arXiv:2011.00387* (2020)
- [20] Xia, C., Wang, J., Qin, Y., Wen, J., Liu, Z., Song, N., Wu, L., Chen, B., Gu, Y., Yang, J.: Karyonet: Chromosome recognition with end-to-end combinatorial optimization network. *IEEE Transactions on Medical Imaging* **42**(10), 2899–2911 (2023)